Transfected plasmid DNA is incorporated into the nucleus via nuclear envelope reformation at telophase

Tokuko Haraguchi (haraguchi@fbs.osaka-u.ac.jp)
Osaka University https://orcid.org/0000-0002-3813-6785

Takako Koujin
National Institute of Communications Technology

Tomoko Shindo
Keio University

Şükriye Bilir
Osaka University

Hiroko Osakada
National Institute of Communications Technology

Kohei Nishimura
Nagoya University

Yasuhiro Hirano
Osaka university https://orcid.org/0000-0001-7339-4053

Haruhiko Asakawa
Osaka University https://orcid.org/0000-0001-9675-658X

Chie Mori
KARC, NICT

Shouhei Kobayashi
NICT

Yasushi Okada
RIKEN Quantitative Biology Center https://orcid.org/0000-0003-2601-3689

Yuji Chikashige
National Institute of Information and Communications Technology

Tatsuo Fukagawa
Osaka University https://orcid.org/0000-0001-8564-6852

Shinsuke Shibata
Keio University School of Medicine https://orcid.org/0000-0002-1185-9043

Yasushi Hiraoka
Osaka University https://orcid.org/0000-0001-9407-8228

Article

Keywords: Transfection, nuclear envelope reformation, telophase, BAF, autophagy, CLEM, iCLEM

Posted Date: July 1st, 2021

DOI: https://doi.org/10.21203/rs.3.rs-478612/v1

Version of Record: A version of this preprint was published at Communications Biology on January 20th, 2022. See the published version at https://doi.org/10.1038/s42003-022-03021-8.

Transfected plasmid DNA is incorporated into the nucleus via nuclear envelope reformation at telophase

Tokuko Haraguchi[1,2,*], Takako Koujin[1,2], Tomoko Shindo[3], Şükriye Bilir[1,], Hiroko Osakada[2,] Kohei Nishimura[1], Yasuhiro Hirano[1], Haruhiko Asakawa[1], Chie Mori[2], Shouhei Kobayashi[2], Yasushi Okada[4,5], Yuji Chikashige[2], Tatsuo Fukagawa[1], Shinsuke Shibata[3,6], Yasushi Hiraoka[1,2]

[1]Graduate School of Frontier Biosciences, Osaka University, 1-3 Yamadaoka, Suita 565-0871, Japan

[2]Advanced ICT Research Institute Kobe, National Institute of Information and Communications Technology, Kobe 651-2492 Japan

[3]Keio University School of Medicine, Shinjuku-ku, Tokyo 160-8582, Japan

[4]RIKEN Center for Biosystems Dynamics Research (BDR), Suita 565-0874, Japan

[5]Universal Biology Institute (UBI) and International Research Center for Neurointelligence (IRCN), the University of Tokyo, Tokyo 113-0033, Japan

[6]Graduate School of Medical and Dental Sciences, Niigata University, Chuo-ku, Niigata 951-8510, Japan

[*]**Corresponding author:**

Tokuko Haraguchi

E-mail: haraguchi@fbs.osaka-u.ac.jp

Phone 81-6-6879-4621

Keywords: Transfection, nuclear envelope reformation, telophase, BAF, autophagy, CLEM, iCLEM

Abstract

DNA transfection is an important technology in the life sciences, wherein nuclear entry of DNA is necessary to achieve expression of the exogenous DNA. Non-viral vectors and their transfection reagents are useful as safe tools for transfection. However, they have no effects for transfection of non-proliferating cells, the reason for which remains unknown. This study aimed to elucidate the mechanism by which transfected DNA enters the nucleus for gene expression. To monitor the intracellular behavior of transfected DNA, we introduced a plasmid bearing *lacO* repeats and RFP-coding sequences into cells expressing GFP-LacI and observed plasmid behavior and RFP expression. RFP expression appeared only after mitosis. Electron microscopy showed that plasmids were wrapped with nuclear envelope (NE)-like membranes or associated with chromosomes at telophase. Depletion of BAF, which is involved in NE reformation, delayed plasmid RFP expression. These results suggest that transfected DNA is incorporated into the nucleus via NE reformation at telophase.

Introduction

Transfection to introduce DNA plasmids into cells is an essential technology in the life sciences and medical fields, for example, in gene therapy. Non-viral vectors and transfection reagents, including cationic lipids or non-liposomal lipids, have been developed as safe tools for introducing exogenous DNA into cells. DNA transfected with these reagents is incorporated into the endosome via endocytosis and exposed to the cytosol upon endosome rupture[1-5], where it is detected by DNA sensor molecules[6-10]. However, it remains unclear how the transfected DNA in the cytosol enters the nucleus. It is empirically known that DNA transfection, which leads to gene expression from foreign DNA, is effective in proliferating cells but not in non-proliferating cells. Therefore, it has been speculated that mitotic events, such as the nuclear envelope (NE) breakdown, are important for nuclear entry of the transfected DNA. However, this has not been experimentally proven yet.

Several attempts have been made to visualize the behavior of transfected DNA and the cellular responses to it[8,11,12]. These include methods using fluorescent dye-conjugated DNA[11], the *lacO*/GFP-LacI visualizing system[11], fluorescent nanodiamond particles coated with DNA[12], and beads conjugated with DNA (DNA-beads)[8]. In the DNA-bead method, it has been shown that DNA-beads are internalized into cells via endocytosis[8,13], entrapped in endosomes, and exposed to the cytosol when the endosome ruptures[8]. Endosome rupture stimulates autophagosome formation in the region of the transfected DNA in a p62-dependent manner[14], leading to its degradation. However, DNA on the beads simultaneously induces NE formation around the DNA-bead in a barrier-to-autointegration factor (BAF)-dependent manner[8]. Once the NE forms around the DNA beads, autophagy is suppressed[8].

BAF is a DNA binding protein[15-18] involved in NE assembly[19-21]. It binds to foreign DNA, such as transfected DNA and viral DNA, in the cytosol[8,15,22-23], where it assembles the NE-like membrane containing LEM domain proteins, such as emerin, around the transfected DNA[8]. This BAF-dependent NE assembly is thought to occur competitively with the assembly of the autophagy membrane[8,24]. However, the biological significance of NE assembly on transfected DNA present in the cytosol is unclear.

The NE is a double-membrane structure consisting of the inner and outer nuclear membranes. The outer membrane is connected to the ER and contains proteins shared with the ER, whereas the inner membrane contains transmembrane proteins specific to the NE. Among the inner nuclear membrane proteins, LEM domain NE proteins, including lamina-associated polypeptide 2 (Lap2), emerin, MAN1, and Lem2, are highly conserved among metazoans[25,26]. LEM domain proteins bind BAF with the LEM domain[19,27-29]. Beneath the inner nuclear membrane, there is a nuclear lamina consisting of lamins[30,31]. There are fenestrated structures, called nuclear pores, spanning the double-membrane structure of the NE[32,33]. The nuclear pore complex (NPC) is formed at the pores. Nucleocytoplasmic transport between the nucleus and cytoplasm is carried out through the NPC.

The NE is disassembled at the beginning of mitosis (prometaphase) and reformed around chromosomes at the end of mitosis (telophase) in higher eukaryotic cells, including human cells. During NE reformation at telophase, emerin and other LEM domain proteins assemble at the “core region” of the chromosome mass in a BAF-dependent manner, whereas lamin B receptor (LBR) and NPC components assemble in the “non-core region” in a BAF-independent manner[19,21,34-36]. The ESCRT-III protein

complex functions to seal gaps in the nuclear membranes during NE reformation at telophase[37].

This study aimed to understand when and how transfected exogenous DNA enters the nucleus. For this purpose, we transfected cells with DNA plasmids designed to visualize the plasmids and monitor their expression. Here, we show that transfected DNA is incorporated into the nucleus when the NE is being reformed during telophase. Our findings will contribute to understanding how foreign DNA behaves within cells, providing useful information for generating improved transfection reagents and techniques.

Results

Protein expression from exogenous DNA occurs only after mitosis

To visualize transfected DNA and its expression, we generated the following experimental system. We constructed a non-viral DNA plasmid (pLacO-pEF1α-mRFP) carrying a *lacO* repeat sequence (256 repeats, about 10 kbp) and a sequence expressing monomeric red fluorescent protein (hereafter RFP) driven by the EF1α promoter (Fig. 1a). We introduced it into human HeLa cells stably expressing EGFP-LacI (hereafter GFP-LacI) using a non-liposomal lipid transfection reagent. Thus, when the DNA plasmid enters the cytosol after endosome rupture, it is visualized by binding to GFP-LacI, forming fluorescent puncta that are easily detected by fluorescence microscopy (Fig. 1a; arrows, Fig. 1b). Plasmid that has not entered the cytosol cannot bind GFP-LacI, and therefore will not be fluorescent (arrowheads, Fig. 1b).

We first assayed efficacy of the GFP-LacI signal to detect transfected exogenous DNA in the cytosol. After removal of transfection reagents, cells were fixed

115 and subjected to indirect immunofluorescence staining using anti-BAF. We examined
116 the overlap between the GFP-LacI signal and BAF, because it is known to bind
117 exogenous DNA immediately after it is released into the cytosol by endosome
118 rupture[8,14,24]. We found that the punctate cytoplasmic GFP-LacI signal, overlapped with
119 that of BAF (Fig. 1b), indicating that our system enabled the visualization of cytosolic
120 plasmid DNA. We also used the DNA-specific fluorescent dye, 4',6-diamidino-2-
121 phenylindole (DAPI), to confirm that the puncta contained DNA. Some of the DAPI
122 puncta did not colocalize with the GFP-LacI signal (arrowheads, upper panels, Fig. 1b),
123 suggesting that some plasmids were retained in endosomes. The GFP-LacI-positive
124 regions of DNA puncta colocalized with the LEM domain NE protein emerin (lower
125 panels, Fig. 1b), suggesting that they were surrounded by an NE-like membrane
126 immediately after release into the cytosol. This result is consistent with the report that
127 DNA-bead complexes become wrapped with NE-like membranes within 5-10 min after
128 endosome rupture[8].
129 We then measured the timing of gene expression from transfected DNA by the
130 appearance of RFP fluorescence (Fig. 1c, d). Time-lapse analysis was carried out
131 immediately after transfection reagents were replaced with culture medium; images
132 were taken every 10 min for 18 h using DeltaVision or LSM880 microscopes. We
133 found that RFP signals appeared only in cells that had proceeded through mitosis (total
134 number of cells tested, n=594) (Fig. 1c, d; Supplementary movies 1, 2), suggesting that
135 gene expression from the transfected plasmid does not occur during interphase before
136 mitosis. RFP expression was detected 2-5 h after the onset of mitotic chromosome
137 segregation (median 150 min, n=594) (Fig. 1d). Since the G1 phase lasts for 6-8 h in the
138 HeLa cell line[38], our data suggest that gene expression occurs during the G1 phase in

most cells (Fig. 1c, d). In these cells, the RFP signal appeared to be comparable in the two daughter cells. However, in a small fraction of the cells, RFP fluorescence appeared later, after 500 min (6 h 20 min). In these cells, the RFP signal often was confined to only one of the daughter cells. The reason for this bias remains unknown.

We also investigated gene expression from transfected DNA in U2OS cells, a human osteosarcoma-derived cell line. We found that gene expression did not occur in pre-mitotic cells, similar to HeLa cells. The timing of gene expression in U2OS cells was 2-5 h (median 150 min) after the onset of chromosome segregation (n = 107) (Supplementary Fig. 1). This median value was the same as that obtained for HeLa cells. These results indicate that gene expression from exogenous DNA transfected using a non-viral transfection reagent occurs only after mitosis in these cell lines. Our findings provide clear evidence for the first time that non-viral transfection is effective only for proliferating cells.

Dynamic behavior of exogenous DNA during mitosis

Protein expression from plasmid DNA did not occur in some cells, even in the presence of GFP-LacI-positive clusters. To understand the difference in the behavior of plasmid DNA between cells with and without gene expression, we characterized the dynamic behavior of GFP-LacI clusters during mitosis. Time-lapse analysis of GFP-LacI in living mitotic cells revealed that in most, GFP-LacI clusters were disjointed at prometaphase with dispersion into smaller puncta during mitosis (Fig. 2a; Supplementary movies 1, 3). In contrast, in some cells, GFP-LacI clusters remained intact during mitosis. Thus, we investigated whether this difference in mitotic behavior was related to gene expression. Most cells with GFP-LacI puncta that dispersed during

mitosis expressed RFP during the subsequent interphase (62 out of 68 cells observed) (Supplementary Fig. 2a), whereas the cells without dispersion did not (6 out of 68 cells) (Supplementary Fig. 2b), suggesting that dispersion of plasmids may be important for gene expression in the subsequent interphase.

We next investigated whether the presence or absence of NE was involved in this GFP-LacI dispersion. Indirect immunofluorescence staining showed that GFP-LacI puncta colocalized with emerin in interphase cells (lower panels, Fig. 1b). In prometaphase cells, in which NE breakdown is ongoing, some of the GFP-LacI puncta colocalized with emerin (arrowheads, upper panels in Fig. 2b), but others did not (lower panels in Fig. 2b). Notably, small puncta (arrows, Fig. 2b') were found near the larger puncta with no emerin signals (lower panels in Fig. 2b; Supplementary Fig. 2c), suggesting that dispersion occurred upon NE breakdown. In metaphase cells, GFP-LacI puncta did not colocalize with emerin (Fig. 2c). Many small puncta of GFP-LacI of the same size were often found in metaphase cells (white puncta, Fig. 2d; Supplementary movie 4). These results suggest that the dispersion of GFP-LacI puncta during mitosis is caused by the breakdown of the NE-like membrane surrounding them. Fig. 2e summarizes the behavior of the GFP-LacI puncta during mitosis.

Plasmid DNA is incorporated into the nucleus via NE reformation at telophase

As gene expression occurs only after mitosis (Fig. 1; Supplementary Fig. 1), we hypothesized that plasmid DNA was incorporated into the nucleus via NE reformation at the end of mitosis. In fact, small puncta of GFP-LacI, probably containing a single copy or a few copies of plasmid DNA, were frequently observed near the telophase chromosomes (arrows, Fig. 3a). To visualize the structural details of these GFP-LacI

puncta, we performed correlative light and electron microscopy (CLEM) on telophase cells undergoing NE reformation (Figs. 3b-f; Supplementary Fig. 3). We selected telophase cells approximately 10 min after the onset of chromosome segregation for CLEM analysis, in which most regions of the chromosomal mass were expected to be surrounded by NE, although some regions may not yet be[21]. At the "core region" of the chromosome mass, the NE containing LEM domain proteins is assembled in a BAF-dependent manner, whereas in the "non-core region", the NE containing LBR and NPC is assembled in a BAF-independent manner (right drawing in Fig. 3a)[19,21,36].

CLEM showed that puncta near the chromosomes at telophase were surrounded by a double-membrane structure similar to the NE or endoplasmic reticulum (ER) (labeled "dot 1" in Figs. 3b, c). This NE-like membrane was fused with the NE on the chromosome (Fig. 3c), suggesting that the transfected DNA is incorporated into the nucleus via membrane fusion. Multiple additional structures were found: dot 2 in Fig. 3d was inside the nucleus (Fig. 3e), while dot 3 was outside and sandwiched between two sets of ER or NE precursor membranes (Fig. 3e). Dot 4 in Fig. 3d was attached to the chromosomes ("Type 4" in Fig. 3f; Supplementary Fig. 3l-o). Relatively larger puncta surrounded by ER or NE precursor membranes were also found in the cytoplasm ("Type 1" in Fig. 3f; Supplementary Fig. 3a-d). We classified these puncta into five types on the basis of their morphologies obtained by CLEM, as indicated in Fig. 3f (also Supplementary Fig. 3): Type 1 (cytoplasmic circle) is a relatively large circular structure covered with a double membrane, which is often found around the GFP-LacI puncta present in the cytoplasm. Type 2 (sandwich) is an electron-dense structure squeezed between two double membranes, suggestive of ER or NE precursor membranes (Fig. 3e; Supplementary Fig. 3e-g). Type 3 (membrane fusion) is a structure

211 in which a relatively large circular structure covered with a double membrane is fused
212 to the NE (Fig. 3c; Supplementary Fig. 3h-k). Type 4 (attached to chromosome) is a
213 structure at the edge of the chromosomal region where the NE is not present
214 (Supplementary Fig. 3l-o). Type 5 (inside the nucleus) is a structure inside the nucleus
215 (between chromosomes) (Supplementary Fig. 3p-s). Besides these types, we frequently
216 observed large GFP-LacI puncta in the cytoplasm. These puncta were found in
217 degradative organelles, including lysosomes and autophagosomes.
218 To confirm the CLEM results, immuno-CLEM analysis was performed using an
219 anti-GFP antibody conjugated with Alexa and nanogold (Fig. 4). GFP-LacI puncta co-
220 stained with Alexa, locating near the telophase chromosome mass, were examined (Fig.
221 4a, b; arrows indicate dots 1-5). Dots 1 and 2 in Fig. 4 were located inside a relatively
222 large circle surrounded by a double membrane structure similar to NE or ER (Fig. 4c),
223 so were classified as type 1. Dot 3 was located on the edge or inside of the
224 chromosomal region (Fig. 4d) and classified as type 4 or 5 (compare with a typical
225 example of Types 4 and 5 in Supplementary Fig. 4). Dots 4 and 5 were located inside
226 the nucleus (Fig. 4e) and were classified as type 5 (compare with a typical example of
227 “Type 5” in Supplementary Fig. 4). These results suggest that at least part of the
228 transfected DNA is attached to the chromosome or located in the nucleus. Therefore,
229 our results suggest that plasmid DNA attaches telophase chromosomes and is
230 subsequently incorporated into the nucleus via NE reformation at the end of mitosis.
231 Fig. 4f shows the typical localization of GFP-LacI puncta at telophase.
232
233 **BAF-dependent NE reformation at telophase facilitates nuclear entry**

To understand the molecular mechanism underlying nuclear entry of exogenous DNA in telophase, we depleted NE proteins and examined the effect on gene expression from the transfected DNA. BAF, emerin and Lem2 were selected as target proteins for depletion because all are known to be involved in NE reformation during telophase[21,39-41]. We first employed the auxin-inducible degron (AID)-induced degradation system to specifically deplete a target protein at the time of interest; for example, only during mitosis[42,43]. For this purpose, we integrated a sequence of mClover3-mAID into each of the three target genes (*BAFN1*, *EMD*, and *LEMD2*) using CRISPR/Cas9 editing[44]. We produced *LEMD2* mutant cell lines (HeLa/mClover3-mAID-Lem2) expressing an mClover3-mAID-Lem2 protein as the sole Lem2 protein (Supplementary Fig. 5), but were not successful for BAF and emerin. Western blotting (WB) of lysates of cells treated with indole-3-acetic acid (IAA) for 60 min showed that Lem2 was almost lost (Supplementary Fig. 5b), consistent with the time-lapse microscopy data (Supplementary Fig. 5c; Supplementary Movie 5).

We examined the effect of Lem2 depletion on exogenous gene expression from the transfected plasmid using time-lapse microscopy (Fig. 5a). The fluorescence of the mClover3-mAID-Lem2 protein was almost completely lost in telophase ("IAA, 0:10" in Fig. 5a) by the addition of IAA in metaphase ("IAA, -1:10" in Fig. 5a), suggesting that depletion of Lem2 worked as expected. Time-lapse analysis of individual cells showed that the timing of gene expression in Lem2-depleted cells was unchanged from that of control cells (Fig. 5b), suggesting that Lem2 does not influence the expression of exogenous DNA at telophase.

Next, we used small interfering RNA (siRNA) treatment to deplete the target proteins. HeLa cells were treated with siRNA against *BAFN1* (iBAF, Fig. 5c-e), with

siRNA against luciferase used as a control (iLuc, Fig. 5c-e). WB showed that the amount of BAF was reduced to 8% under these conditions (Fig. 5d). Then, cells depleted of BAF were transfected with the plasmid and gene expression was assessed in individual cells by fluorescence microscopy (Fig. 5c). The timing of gene expression in cells treated with *BAFN1* siRNA (median 180 min, n=136) was delayed relative to that of the control cells (median 140 min, n=129) (Fig. 5e). To confirm that BAF was truly depleted in the cells assayed by microscopy, a similar experiment was carried out using cells expressing GFP-BAF, which produced similar results (Supplementary Fig. 6a, b). Because BAF is known to be required for NE reformation at telophase[21], these data suggest that NE reformation during telophase is an important step for the entry of exogenous DNA into the nucleus**.** We also tested the effect of emerin siRNA depletion, but it has no effect on the timing of gene expression (Supplementary Fig. 6c-e).

NE rupture can cause pre-mitotic gene expression from exogenous DNA

Our data led us to hypothesize that intact NE in interphase cells blocks the entry of foreign DNA into the nucleus. To test this hypothesis, we physically ruptured the NE, then examined whether gene expression occurred from exogenous DNA without telophase NE reformation. To do this, cells were transfected with plasmids. Immediately after removal of the transfection reagent, the transfected cells were microinjected with FITC-dextran to rupture the NE. FITC-dextran was used as a marker for the NE rupture (Fig. 6a). Time-lapse microscopy showed that some of the NE-ruptured cells expressed RFP from plasmid DNA, even in interphase cells that had never undergone mitosis (Fig. 6b). Similarly, premitotic gene expression from transfected DNA was observed in cells depleted of NE proteins. When emerin was

depleted with siRNA treatment, premitotic gene expression from the transfected DNA was observed (5 of 131 cells tested; Fig. 6c, d). No premitotic gene expression was observed in the control siRNA treatment (129 cells tested; Supplementary Fig. 6e). These results demonstrate that transient NE rupture caused by physical punctation or depletion of the NE proteins allowed nuclear entry of the transfected DNA, resulting in gene expression from foreign DNA, even in premitotic cells.

Discussion

Multiple cellular barriers to the delivery of DNA plasmids to the nucleus are known to exist, including intracellular uptake, endosome acidification, autophagy, immune sensing pathways, and nuclear entry[45,46]. This study focused on how transfected DNA enters the nucleus. We found that gene expression occurs only after telophase, with plasmids associated with telophase chromosomes enwrapped by the NE. Therefore, we concluded that NE reformation at telophase is important for the nuclear entry of the transfected DNA. This conclusion indicates that NE acts as a physical barrier to the delivery of foreign DNA into the nucleus, and that NPC-mediated nuclear transport of foreign DNA does not occur in interphase cells. If premitotic gene expression happened to occur in interphase cells, transient NE rupture might have been induced in these cells. This hypothesis is consistent with our data showing that premitotic gene expression occurs in cells in which the NE has been ruptured by a microinjection needle (Fig. 6a, b), and in cells in which emerin and BAF were depleted (Fig. 6c, d). Similar transient NE ruptures have been reported in some diseases, including laminopathy and cancers[47,48]. In addition, BAF has been reported to play a role to repair NE rupture[49], consistent with our finding.

306 It has been reported that most plasmids form clusters in the cytosol after
307 endosomal escape, regardless of transfection method; moreover, the clusters are
308 relatively immobile during interphase[11]. The clusters remaining at metaphase are
309 asymmetrically partitioned with a bias to the younger centrosomes in dividing cells[11].
310 We also found similar plasmid clusters in the cytosol. However, most of them were
311 dispersed at the beginning of mitosis to smaller puncta. The small puncta were scattered
312 throughout the cell and distributed to daughter cells (Fig. 2a; Supplementary movies 1
313 and 3), whereas the large puncta were retained in one cell as reported previously[11].
314 Because gene expression from foreign DNA occurred only in cells with small puncta,
315 the small puncta that are incorporated into the reassembling nucleus at telophase are
316 associated with efficient gene expression from foreign DNA in the G1 phase. The
317 biological significance of plasmid clusters in mitosis remains unclear.
318 Transfected DNA in the cytosol activates DNA sensor signaling pathways[6,7,50].
319 Binding of DNA sensors to the cytosolic DNA is hypothesized to be a defense response
320 against infection. Many DNA sensor proteins have been identified, including cyclic
321 GMP-AMP synthase (cGAS)[51] and their common signaling adaptor stimulator of
322 interferon (IFN) gene (STING)[52], DNA-dependent activator of interferon regulatory
323 factors/Z-DNA binding protein 1 (DAI/ZBP1)[53], interferon activated gene 204 (p204)[54],
324 DEAD box helicase 60 (DDX60)[55], and BAF[8,24]. DAI/ZBP1 and p204 have been
325 reported to bind cytosolic plasmid DNA within 15 min, whereas DDX60 does not[56].
326 BAF binds the cytosolic DNA within seconds[8] and plays a role in assembling the NE-
327 like membrane around the plasmid DNA within approximately 10 min[8]. This BAF-
328 dependent NE assembly protects foreign DNA from autophagy[8,24]. Although BAF is
329 expected to function as a defense against viral infection[23,57,58], it unexpectedly assists in

the integration of the human immunodeficiency virus (HIV) genome into the host genome[15,16]. In addition, a recent report showed that BAF protects against the cGAS-STING response to prevent innate immune activation[59,60]. Collectively, these data suggest that BAF can suppress the innate immune response and act to safely carry the cytosolic DNA to the next cell cycle stages by wrapping it in the NE-like membrane.

In summary, our data suggest that NE acts as a barrier for foreign DNA to enter the nucleus, and that foreign DNA is incorporated into the nucleus when the NE is being reassembled in telophase. Our findings provide important insights not only for understanding cellular responses during DNA transfection, but also for the development of transfection reagents and methods.

Materials and Methods

Plasmids. We constructed the plasmid carrying a *lacO* repeat sequence and a sequence expressing RFP driven by the EF1α promoter (pLacO-pEF1α-mRFP) as follows: First, to generate the mRFP-C1 vector, the DNA fragment encoding mRFP was amplified by PCR from the mRFP-pRSETB vector using the primer set mRFP-FWD3-Nhe (5'-GAGCTAGCATGGCCTCCTCCGAGGACGTCA-3') and mRFP-REV2-Bgl (5'-TAAGATCTGGCGCCGGTGGAGTGGCGGCCC-3'), and the PCR product was inserted into the pEGFP-C1 vector (Clontech, Takara Bio Inc., Kusatsu, Japan) at the *Nhe*I and *Bgl*II sites. The resulting plasmid is called the mRFP-C1 vector. Next, to generate the pEF1α-mRFP plasmid, the DNA fragment encoding the EF1α-promoter region was amplified by PCR from the pBOS-H2B-GFP vector (Stratagene, La Jolla, CA) using the primers EF1α-prom.FWD-Ase (5'-GGGATTAATCGTGAGGCTCCGGTGCCCGTCAGTGG-3') and EF1α-prom.REV-

Nhe (5’-GGGCTAGCCTCACGACACCTGAAATGGAAGAAAAAAACTTTG-3’) , and the PCR product was inserted into the mRFP-C1 vector at the *Ase*I and *Nhe*I sites. The resulting plasmid is called the pEF1α-mRFP plasmid. Then, the pEF1α-mRFP plasmid was digested with *Sal*I, then circularized with a ligation kit (Ligation High Ver.2, Toyobo Co., Osaka, Japan) after filling the gaps with *E. coli* DNA polI Klenow fragment (Takara Bio Inc., Kusatsu, Japan) to generate the pEF1α-mRFP-C1-ΔSalI vector. The pEF1α-mRFP-C1-ΔSalI vector was inserted with the sequence of TAGTCGAC to generate a new *Sal*I site in front of the EF1α promoter region to generate the SalI-pEF1α-mRFP-C1 vector. Finally, to generate pLacO-pEF1α-mRFP, the DNA fragment containing a *LacO*-repeat sequence was obtained by digestion of the pSV-dhfr DNA plasmid, then inserted into the SalI-pEF1α-mRFP-C1 vector at its *Sal*I site using Ligation High Ver.2 (Toyobo Co., Osaka, Japan).

To construct the plasmid expressing EGFP-fused LacI (GFP-LacI), EGFP was amplified by PCR from the pEGFP-C1 vector (Clontech, Takara Bio Inc., Kusatsu, Japan) using the primers 5’-TGTGACCGGGCGCCTACTATGGTGAGCAAGGGCGAGGAGCT-3’ and 5’-CGAATTCGCTAGCTCTAGACTTGTACAGCTCGTCCATGC-3’, and the PCR product was inserted into the PB-EF1α-MCS-IRES-Neo vector (PB533A-2, System Biosciences, Mountain View, CA, USA) using *Xba*I sites to generate the PB-EF1α-EGFP-MCS-IRES-Neo vector. Next, DNA encoding LacI was amplified from the MK9-38/pYC19 vector using the primers (5’-ATTCGAATTTAAATCGGATATGGTGAAACCAGTAACGTTATA-3’ and 5’-CTCAGCGGCCGCGGATCTTACAGCTGCATTAATGAATCGGCC-3’) and the

377 PCR product was inserted into the PB-EF1α-EGFP-MCS-IRES-Neo vector using a
378 *Bam*HI site to generate the plasmid expressing GFP-LacI.
379
380 **Cell strains and culture.** HeLa and U2OS cells were obtained from the Riken Cell
381 Bank (RCB007, Tsukuba, Japan) and the Health Protection Agency (London, UK),
382 respectively. To generate HeLa cells stably expressing GFP-LacI (HeLa/GFP-LacI),
383 they were transfected with plasmids encoding GFP-LacI using Effectene (Qiagen,
384 Hilden, Germany), according to the manufacturer's instructions. Cells were selected
385 with 800 μg/ml Geneticin (11811-031, Life Technologies, Thermo Fisher Scientific,
386 Tokyo, Japan). Several clones were isolated from the survivors and their expression
387 levels were evaluated using WB. The selected clones were maintained in DMEM
388 containing 10% fetal bovine serum (FBS) and 200 μg/ml Geneticin (11811-031, Life
389 Technologies, Thermo Fisher Scientific, Tokyo, Japan). We established *LEMD2* mutant
390 cell lines (HeLa/mClover3-mAID-Lem2) expressing an mClover3-mAID-Lem2 protein
391 as the sole Lem2 protein as describe below (see section "Depletion of NE proteins" in
392 Materials and Methods).
393
394 **Antibodies.** Primary mouse monoclonal antibodies included anti-GFP for indirect
395 immunofluorescence staining and WB (Cat No. 632381, Lot No. 1004037, Clontech,
396 USA), anti-α-tubulin (clone DM1A, Cat No. T9026, Lot No. 017H4838, Sigma), and
397 anti-BAF for WB (BANF1, Cat No. H00008815-M01, Lot No. 6132-S3, Abnova,
398 Taipei, Taiwan). Primary rabbit polyclonal antibodies included anti-GFP antibody for
399 iCLEM (Cat No. 600-401-215, Lot No. 24437, Rockland, Limerick, PA, USA), anti-
400 emerin (ED1)[61], anti-BAF (PU38143)[62], anti-Lem2 (LEMD2, Cat No. HPA017340, Lot

No. B96759, Atlas Antibodies, Bromma, Sweden), and anti-β-actin (Cat No. ab8227, Lot No. GR14272-3, Abcam). Alexa594-conjugated secondary antibodies against mouse IgG (Cat No. A11037, Thermo Fisher Scientific) and rabbit IgG (Cat No. A11032, Thermo Fisher Scientific) were used to detect the primary antibodies.

Transfection and live-cell imaging. HeLa/GFP-LacI cells were seeded on 35-mm glass-bottom culture dishes (MatTek, MA, USA) at a concentration of 2 x 10^5 per dish one day before imaging. For transfection, the cells were incubated for 4 h with Effectene transfection reagent (Qiagen) containing 0.5 μg/dish pLacO-pEF1α-mRFP. During this incubation, Hoechst 33342 was added to a final concentration of 100 ng/ml and incubated for 15 min to stain DNA. After transfection reagents were replaced with culture medium, cells were subjected to time-lapse imaging. Images for each wavelength were obtained every 10 min (1 μm × 7 z-stacks for a single time point unless otherwise specified) through an oil-immersion objective lens UApo/340 (40x, NA = 1.35, Olympus, Tokyo, Japan) using the DeltaVision fluorescence microscope system (GE Healthcare Japan, Tokyo, Japan) in a temperature-controlled (37°C) room; this microscope system is equipped with a high-sensitive sCMOS camera (pico.edge 4.2, PCP AG, Kelheim, Germany). Images were also obtained every 10 min (2 μm x 5 z-stacks for a single time point) through a water-immersion objective lens C-Apo40 (40x, NA=1.2, Carl Zeiss, Jena, Germany) on a confocal fluorescence microscope system LSM880 (Carl Zeiss), maintained at 37°C using a stage warmer. Scanning conditions were as follows: pinhole size 2.5 A.U.; laser power 0.5-1%; zoom 1; scan speed 6; averaging 2; tiling 5 × 5.

Immunofluorescence staining. HeLa/GFP-LacI cells were transfected with plasmid using Effectene as described above. Immediately after removal of the transfection reagent, cells were fixed with a fixative (3.7% formaldehyde and 0.2% glutaraldehyde in PBS) and incubated with anti-BAF or anti-emerin antibodies as previously described[19,62]. Anti-rabbit IgG-conjugated Alexa-594 was used as the secondary antibody. Fluorescence images were obtained using an Olympus oil-immersion objective lens PLAPON60xOSC (NA = 1.40) on the DeltaVision microscope system. Z-stacks of images (typically 20-30 focal planes at 0.5 μm intervals) were obtained and deconvoluted using software provided with the microscope system, SoftWorx.

Super-resolution microscopy. HeLa/GFP-LacI cells were transfected with plasmid using Effectene as described above. After removal of the transfection reagent, cells were fixed with a fixative (3.7% formaldehyde and 0.2% glutaraldehyde in PBS). Then, cells were observed by LSM880 Airyscan system (Carl Zeiss) equipped with Plan-Apochromat 63x/1.40 M27 objective lens using immersion oil (#518F, Carl Zeiss) at room temperature (RT, approximately 26°C). Pinhole size was set to 384 μm. Hoechst and GFP were excited with 405 and 488 nm laser, respectively. The fluorescent signals for Hoechst and GFP were collected using the following beam splitters and bandpass filters: MBS-405 and BP 420-480 for Hoechst and MBS488/561 and BP 495-550 for GFP. Images were acquired at 988 pixels each with 0.037 μm/pixel. A z-stack image set was acquired for 133 focal planes with 0.159 μm intervals. After processing for super-resolution image, brightness and contrast were changed for better visibility in Zen 2.3 SP1 software without changing gamma.

Correlative light and electron microscopy (CLEM). HeLa/GFP-LacI cells were transfected with plasmid using Effectene as described above. After removal of the transfection reagent, cells were fixed with 2.5% glutaraldehyde for 1 h. CLEM was performed with some modifications of our previously published method[21]. Briefly, after washing with PBS, the telophase cells 8-10 min after metaphase to anaphase transition were selected by morphology, then subjected to fluorescence microscopy (FM) to obtain 3D images (typically 40-60 focal planes at 0.2 μm intervals) using a low-chromatic-aberration oil-immersion lens PLAPON60xOSC (NA = 1.40, Olympus) on a DeltaVision microscope system. The images were deconvoluted to remove out-of-focus images using software provided with the microscope system. Samples were post-fixed with 1% OsO_4 (3002, Nisshin EM, Tokyo, Japan), stained with 2% uranyl acetate (8473-1M, Merck, Darmstadt, Germany), and then embedded in Epon812 (T024, TAAB, England). Cells observed by FM were identified in the block. Ultrathin sections of 80 nm were prepared and further stained with 4% uranyl acetate, followed by a commercial ready-to-use solution of lead citrate (18-0875-2, Sigma-Aldrich, St. Louis, MO, USA). Electron microscopy (EM) images were acquired using a JEM-1400 electron microscope (80 kV; JEOL, Tokyo, Japan). To correlate the FM and EM images, we selected the FM image corresponding to the EM image from the 3D FM images by eye using criteria including nuclear shapes and areas of bead cross-sections.

Immuno-CLEM (iCLEM). HeLa/GFP-LacI cells were transfected for 4 h with 0.2 μg/dish pLacO-pEF1α-mRFP using Effectene as described above. After removal of transfection reagents, cells were fixed with a mixture of 3.7% formaldehyde and 0.2% glutaraldehyde for 15 min. After washing with PBS, cells were permeabilized with

0.01% Triton X-100 in PBS for 5 min at RT (26°C), treated twice with 0.1% sodium borohydride in PBS for 15 min, and washed twice with 1% BSA in PBS for 1 h. Cells were then incubated with anti-GFP antibody (1:500 dilution in 1% BSA in PBS, 600-401-215, lot. No. 35459, Rockland). After extensive washing with PBS (10 min × 12 times), cells were incubated with a secondary Alexa594-nanogold-anti rabbit antibody (1:200 dilution in 1% BSA in PBS, Nanoprobes, Yaphank, NY, USA) for 3 h at RT. A z-stack of fluorescence images (typically 40–60 focal planes at 0.2-μm intervals) were acquired for cells of interest using a low-chromatic-aberration PLAPON60xOSC (NA = 1.40) objective on a DeltaVision microscope system as described above. Then, cells were fixed with 1% glutaraldehyde for 1 h and washed with PBS three times. After washing twice with 100 mM Lysine-HCl/PB (pH 7.4) for 10 min, cells were subjected to silver enhancement as follows: cells were washed with PBS, incubated with 50 mM HEPES (pH 5.8) three times, and washed with distilled water. Cells were then treated with silver-enhancing reagent at 25°C for 5 min and washed with distilled water three times. Samples were post-fixed with 1% OsO_4 (3002, Nisshin EM), stained with 2% uranyl acetate (8473-1M, Merck), and embedded in Epon812 (T024, TAAB) as described previously[21]. Cells observed by fluorescence microscopy were identified in the block. Ultrathin sections with a thickness of 80 nm were prepared and further stained with 4% uranyl acetate (8473-1M, Merck), followed by a commercial ready-to-use solution of lead citrate (18-0875-2, Sigma-Aldrich). EM images were acquired using a JEM-1400 plus electron microscope (80 kV; JEOL, Tokyo, Japan). To correlate the FM and EM images, we selected FM image corresponding to EM images from the 3D FM images by eye, using criteria including nuclear shape and area of bead cross-section in each image.

Depletion of NE proteins. To deplete BAF, HeLa cells or HeLa cells stably expressing GFP-BAF were treated with *BAFN1* siRNA (Qiagen) using RNAiMax (Thermo Fisher Scientific) as described previously[21]. To deplete emerin, HeLa cells were treated with *EMR* siRNA [AACCGTGCTCCTGGGGCTGGG, Qiagen][63] using RNAiMax. Luciferase siRNA (Qiagen) was used as the negative control.

The AID-induced protein degradation system was used to deplete Lem2 as described previously[43]. The plasmid pAID1.2-EF1a-NmClover3-mAID, was developed from pAID1.2-EF1a-NGFP-mAID (Addgene plasmid #140607). The cDNA sequence of Lem2 was amplified by PCR and cloned into the pAID1.2-EF1a-NmClover3-mAID vector at the *Eco*RV site using the In-Fusion HD Cloning Kit (Takara Bio Inc.). The pX330 plasmid targeting the human *LEMD2* gene was constructed as described previously[44]. The sequence 5'-GACTTACTCACCAGCTTGGATGG-3' at the intron-exon boundary of the 3' end of exon 3 of the human *LEMD2* gene was selected as a target for CRISPR/Cas9-mediated gene editing. These plasmids were cotransfected with pAID EF1a linearized in pX330 (plasmid #140610, Addgene) into HeLa cells. After selection in 8 μg/ml blasticidin S (029-18701, Wako, Osaka, Japan), several clones were picked; their expression levels of endogenous and mClover3-mAID-tagged Lem2 were evaluated by WB using anti-Lem2 and anti-GFP antibodies, respectively. We used an anti-GFP antibody to detect mClover3-mAID-Lem2 because the anti-GFP antibody could cross-react with mClover3. AID-mediated protein degradation was induced by adding final 0.5 mM indole-3-acetic acid (IAA).

520 **Western Blotting (WB).** WB was performed as previously described[62]. Briefly, cells
521 were collected and lysed in ice-cold isotonic buffer (20 mM Tris-HCl, pH 7.5, 2 mM
522 $MgCl_2$, 150 mM NaCl, 0.5% NP-40, Protease Inhibitor Cocktail) (final 1×10^7
523 cell/ml). Equal amounts of 2x SDS-PAGE sample buffer (without DTT) were added
524 to the lysates. After sonication, the lysates were boiled for 5 min. DTT (freshly
525 prepared from powder) was added to the samples at a final concentration of 20 mM.
526 Ten micrograms of total protein from the cell extract were loaded into each lane of an
527 SDS 10–20% gradient polyacrylamide gel or 15% polyacrylamide gel. After
528 electrophoresis, proteins were transferred to PVDF membranes using a semi-dry
529 blotting system (Atto Corp., Tokyo, Japan) and stained using the ECL western blotting
530 detection system (GE Healthcare).
531
532 **NE rupture.** HeLa/GFP-LacI cells were transfected using the transfection reagent
533 Effectene (Qiagen) with 0.3 μg/dish of pLacO-pEF1α-mRFP for 3 h. During this
534 incubation, Hoechst 33342 was added to a final concentration of 100 ng/ml and
535 incubated for 15 min to stain DNA. After removal of the transfection mixture, the
536 culture medium was replaced with fresh DMEM containing 10% FBS and then
537 subjected to fluorescence imaging. Cells in the glass-bottom culture dish were placed on
538 a stage of the DeltaVision fluorescence microscope in a temperature-controlled room
539 (37°C). Cells of interest, i.e., the cells appearing to be undergoing G1 phase, were
540 selected based on the morphology observed via bright-field microscopy; their NEs were
541 disrupted using the tip of a microinjection needle (Femtotips, Eppendorf, No.
542 5242952008 Eppendorf, Hamburg, Germany) attached to a microinjector (microinjector
543 5242 and micromanipulator 5171, Eppendorf). To confirm NE rupture, cells were

concomitantly microinjected with 0.5 μg/μl FITC-dextran (MW, 10 kDa) as an injection marker. Fluorescence images were obtained at 10-15 min intervals for 4 h.

Data availability

The authors declare that the data supporting the findings of this study are available within the paper and its supplementary information files. The source data underlying Fig. 1d, 5b, 5e, Supplementary Fig. 1, 6b, and 6e are provided as a source data file. Further data are available from the corresponding authors upon request.

References

1. Conner, S. D., & Schmid, S. L. Regulated portals of entry into the cell. *Nature* 422, 37-44. doi: 10.1038/nature01451 (2003).
2. Hoekstra, D., Rejman, J., Wasungu, L., Shi., F, & Zuhorn, I. Gene delivery by cationic lipids: in and out of an endosome. *Biochem. Soc. Trans.* **35**, 68-71. doi: 10.1042/BST0350068 (2007).
3. Zylberberg, C., Gaskil, K., Pasley, S., Matosevic, S. Engineering liposomal nanoparticles for targeted gene therapy. *Gene Ther.* **24**, 441-452. doi: 10.1038/gt.2017.41 (2017).
4. Brock DJ, Kondow-McConaghy HM, Hager EC, Pellois JP. Endosomal Escape and Cytosolic Penetration of Macromolecules Mediated by Synthetic Delivery Agents. *Bioconjugate Chem.* **30**, 293-304. doi: 10.1021/acs.bioconjchem.8b00799 (2019).
5. Ita K. Polyplexes for gene and nucleic acid delivery: Progress and bottlenecks. *Eur. J. Pharm. Sci.* **150**, 105358. doi: 10.1016/j.ejps.2020.105358 (2020).
6. Takaoka, A., & Taniguchi, T. Cytosolic DNA recognition for triggering innate immune responses. *Adv. Drug Deliv. Rev.* **60**, 847-57. doi:10.1016/j.addr.2007.12.002 (2008).
7. Yanai, H., Savitsky, D., Tamura, T., & Taniguchi, T. Regulation of the cytosolic DNA-sensing system in innate immunity: a current view. *Curr. Opin. Immunol.* **21**, 17-22. doi: 10.1016/j.coi.2009.01.005 (2009).
8. Kobayashi, S. et al. BAF is a cytosolic DNA sensor that leads to exogenous DNA avoiding autophagy. *Proc. Natl. Acad. Sci. USA* **112**, 7027-7032. doi: 10.1073/pnas.1501235112 (2015).

9. Chen, Q., Sun, L., & Chen, Z. J. Regulation and function of the cGAS-STING pathway of cytosolic DNA sensing. *Nat. Immunol.* **17**, 1142-9. doi: 10.1038/ni.3558 (2016).
10. Hopfner, K. P., & Hornung, V. Molecular mechanisms and cellular functions of cGAS-STING signalling. *Nat. Rev. Mol. Cell Biol.* **21**, 501-521. doi: 10.1038/s41580-020-0244-x (2020).
11. Wang, X., Le, N., Denoth-Lippuner, A., Barral, Y., & Kroschewski, R. Asymmetric partitioning of transfected DNA during mammalian cell division. *Proc. Natl. Acad. Sci. USA* **113**, 7177-82. doi: 10.1073/pnas.1606091113 (2016).
12. Petrakova, V., Benson, V., Buncek, M., Fiserova, A., Ledvina, M., Stursa, J., Cigler, P., & Nesladek, M. I Imaging of transfection and intracellular release of intact, non-labeled DNA using fluorescent nanodiamonds. *Nanoscale* **8**, 12002-12. doi: 10.1039/c6nr00610h.PMID: 27240633 (2016).
13. Kobayashi, S., Kojidani, T., Osakada, H., Yamamoto, A., Yoshimori, T., Hiraoka, Y., & Haraguchi, T. Artificial induction of autophagy around polystyrene beads in nonphagocytic cells. *Autophagy* **6,** 36-45 (2010).
14. Tsuchiya, M., Ogawa, H., Koujin, K., Kobayashi, S., Mori, C., Hiraoka, Y., & Haraguchi, T. Depletion of autophagy receptor p62/SQSTM1 enhances the efficiency of gene delivery in mammalian cells. *FEBS Lett.* **590**, 2671-80. doi: 10.1002/1873-3468.12262 (2016)
15. Lee, M. S., & Craigie, R. A previously unidentified host protein protects retroviral DNA from autointegration. *Proc. Natl. Acad. Sci. USA* **95**, 1528-1533. doi:10.1073/pnas.95.4.1528 (1998).

16. Chen, H. & Engelman, A. The barrier-to-autointegration protein is a host factor for HIV type 1 integration. *Proc. Natl. Acad. Sci. USA* **95**, 15270-15274. doi:10.1073/pnas.95.26.15270 (1998).
17. Umland, T. C., Wei, S.-Q., Craigie, R. & Davies, D. R. Structural basis of DNA bridging by barrier-to-autointegration factor. *Biochemistry* **39**, 9130-9138. doi:10.1021/bi000572w (2000).
18. Zheng, R., Ghirlando, R., Lee, M. S., Mizuuchi, K., Krause, M. & Craigie, R. Barrier-to-autointegration factor (BAF) bridges DNA in a discrete, higher order nucleoprotein complex. *Proc. Natl. Acad. Sci. USA* **97**, 8997-9002. doi:10.1073/pnas.150240197 (2000).
19. Haraguchi, T., Koujin, T., Segura-Totten, M., Lee, K. K., Matsuoka, Y., Yoneda, Y., Wilson, K. L., & Hiraoka, Y. BAF is required for emerin assembly into the reforming nuclear envelope. *J. Cell Sci*. **114**, 4575-4585 (2001).
20. Gorjánácz, M., Klerkx, E. P., Galy, V., Santarella, R., López-Iglesias, C., Askjaer, P. & Mattaj, I. W. Caenorhabditis elegans BAF-1 and its kinase VRK-1 participate directly in post-mitotic nuclear envelope assembly. *EMBO J.* **26**, 132-143. doi:10.1038/sj.emboj.7601470 (2007).
21. Haraguchi, T., Kojidani, T., Koujin, T., Shimi, T., Osakada, H., Mori, C., Yamamoto, A., & Hiraoka, Y. Live cell imaging and electron microscopy revealed dynamic processes of BAF-directing nuclear envelope assembly. *J. Cell Sci.* **121**, 2540-2554. doi: 10.1242/jcs.033597 (2008)
22. Wiebe, M. S., & Traktman, P. Poxviral B1 kinase overcomes barrier to autointegration factor, a host defense against virus replication. *Cell Host Microbe* **1**, 187-197. doi:10.1016/j.chom.2007.03.007 (2007).

623 23. Ibrahim, N, Wicklund, A, Jamin, A, Wiebe, M. S. Barrier to autointegration factor
624 (BAF) inhibits vaccinia virus intermediate transcription in the absence of the viral
625 B1 kinase. *Virology* **444**, 363-73. doi: 10.1016/j.virol.2013.07.002 (2013).
626 24. Kobayashi, S., & Haraguchi, T. A novel pathway to detect and cope with
627 exogenous dsDNA. *Commun. Integr. Biol.* **8**, e1065361,
628 doi:10.1080/19420889.2015.1065361 (2015).
629 25. Wagner, N., & Krohne, G. LEM-domain proteins: new insights into lamin-
630 interacting proteins. *Int. Rev. Cytol.* **261**, 1–46 (2007).
631 26. Brachner, A., & Foisner, R. Evolvement of LEM proteins as chromatin tethers at
632 the nuclear periphery. *Biochem. Soc. Trans.* **39**, 1735-1741.
633 doi:10.1042/BST20110724 (2011).
634 27. Cai, M., Huang, Y., Ghirlando, R., Wilson, K. L., Craigie, R., & Clore, G.M.
635 Solution structure of the constant region of nuclear envelope protein LAP2 reveals
636 two LEM-domain structures: one binds BAF and the other binds DNA. *EMBO J.*
637 **20**, 4399-407. doi: 10.1093/emboj/20.16.4399 (2001).
638 28. Lee, K. K., Haraguchi, T., Lee, R. S., Koujin, T, Hiraoka, Y., & Wilson, K. L.
639 Distinct functional domains in emerin bind lamin A and DNA-bridging protein
640 BAF. *J. Cell Sci.* **114**, 4567-73 (2001).
641 29. Shumaker, D. K., Lee, K. K., Tanhehco, Y. C., Craigie, R., & Wilson, K. L. LAP2
642 binds to BAF.DNA complexes: requirement for the LEM domain and modulation
643 by variable regions. *EMBO J.* **20**, 1754-64. doi: 10.1093/emboj/20.7.1754 (2001).
644 30. Moir, R. D., & Goldman, R. D. Lamin dynamics. *Curr. Opin. Cell Biol.* **5**, 408-11.
645 doi: 10.1016/0955-0674(93)90004-a (1993).

646 31. Tenga, R., & Medalia, O. Structure and unique mechanical aspects
647 of nuclear lamin filaments. *Curr. Opin. Struct. Biol.* **64**, 152-159. doi:
648 10.1016/j.sbi.2020.06.017 (2020).
649 32. Hampoelz, B., Andres-Pons, A., Kastritis, P., & Beck, M. Structure and Assembly
650 of the Nuclear Pore Complex. *Annu. Rev. Biophys.* **48**, 515-536. doi:
651 10.1146/annurev-biophys-052118-115308 (2019).
652 33. Bilir, Ş., Kojidani, T., Mori, C., Osakada, H., Kobayashi, S., Koujin, T., Hiraoka,
653 Y., & Haraguchi, T. *Genes Cells* **24**, 338-353. doi: 10.1111/gtc.12677 (2019).
654 34. Shimi, T., Koujin, T., Segura-Totten, M., Wilson, K. L. Haraguchi, T. & Hiraoka,
655 Y. Dynamic interaction between BAF and emerin revealed by FRAP, FLIP and
656 FRET analyses in living HeLa cells. *J. Struct. Biol.* **147**, 31-41 (2004).
657 35. Dechat, T., Gajewski, A., Korbei, B., Gerlich, D., Daigle, N., Haraguchi, T.,
658 Furukawa, K., Ellenberg, J., & Foisner, R. LAP2alpha and BAF transiently localize
659 to telomeres and specific regions on chromatin during nuclear assembly. *J. Cell Sci.*
660 **117**, 6117-28. doi: 10.1242/jcs.01529. (2004).
661 36. Clever, M., Mimura, Y., Funakoshi, T., & Imamoto, N. Regulation and
662 coordination of nuclear envelope and nuclear pore complex assembly. *Nucleus* **4**,
663 105-14. doi: 10.4161/nucl.23796 (2013).
664 37. Olmos, Y., Hodgson, L., Mantell, J., Verkade, P., & Carlton, J.G. ESCRT-III
665 controls nuclear envelope reformation. *Nature* **522**, 236-9. doi:
666 10.1038/nature14503 (2015).
667 38. Haraguchi, T., Kaneda, T., & Hiraoka, Y. Dynamics of chromosomes and
668 microtubules visualized by multiple-wavelength fluorescence imaging in living

669 mammalian cells: effects of mitotic inhibitors on cell cycle progression. *Genes*
670 *Cells* **2**, 369-80. doi:10.1046/j.1365-2443.1997.1280326.x (1997).
671 39. Asencio, C., Davidson, I. F., Santarella-Mellwig, R., Ly-Hartig, T. B., Mall, M.,
672 Wallenfang, M. R., Mattaj, I. W., & Gorjánácz, M. Coordination of kinase and
673 phosphatase activities by Lem4 enables nuclear envelope reassembly
674 during mitosis. *Cell* **150**, 22-35. doi: 10.1016/j.cell.2012.04.043 (2012).
675 40. von Appen, A., LaJoie, D., Johnson, I. E., Trnka, M. J., Pick, S. M., Burlingame, A.
676 L., Ullman, K. S., & Frost, A. LEM2 phase separation promotes ESCRT-mediated
677 nuclear envelope reformation. *Nature* **582**, 115-118. doi: 10.1038/s41586-020-
678 2232-x (2020).
679 41. Dubińska-Magiera, M., Kozioł K, Machowska M, Piekarowicz K, Filipczak D,
680 Rzepecki R. Emerin Is Required for Proper Nucleus Reassembly after Mitosis:
681 Implications for New Pathogenetic Mechanisms for Laminopathies Detected in
682 EDMD1 Patients. *Cells* **8**, 240. doi: 10.3390/cells8030240 (2019).
683 42. Nishimura, K., & Fukagawa T. An efficient method to generate conditional
684 knockout cell lines for essential genes by combination of auxin-inducible degron
685 tag and CRISPR/Cas9. *Chromosome Res.* **25**, 253-260. doi: 10.1007/s10577-017-
686 9559-7 (2017).
687 43. Nishimura, K., Yamada, T., Hagihara, S., Iwasaki, R., Uchida, N., Kamura, T.,
688 Takahashi, K., Torii, K. U. & Fukagawa, T. A super-sensitive auxin-inducible
689 degron system with an engineered auxin-TIR1 pair. *Nucleic Acids Res.* **48**, e108.
690 doi: 10.1093/nar/gkaa748 (2020).

691 44. Pyzocha, N. K., Ran, F. A., Hsu, P. D., & Zhang, F. RNA-guided genome editing
692 of mammalian cells. *Methods Mol. Biol.* **1114**, 269-277. doi: 10.1007/978-1-62703-
693 761-7_17 (2014).
694 45. Olden, B. R., Cheng, E., Cheng, Y., & Pun, S. H. Identifying key barriers in
695 cationic polymer gene delivery to human T cells. *Biomater. Sci.* **7**, 789-797. doi:
696 10.1039/c8bm01262h (2019).
697 46. Nguyen, J., & Szoka, F. C. Nucleic acid delivery: the missing pieces of the puzzle?
698 *Acc. Chem. Res.* **45**, 1153-62. doi: 10.1021/ar3000162 (2012).
699 47. Houthaeve, G., Robigins, J., Braeckmans, K., & De Vos, W. H. Bypassing Border
700 Control: Nuclear Envelope Rupture in Disease. *Physiology* (Bethesda) **33**, 39-49.
701 doi: 10.1152/physiol.00029.2017 (2018).
702 48. Lim, S., Quinton, R. J., & Ganem, N. J. Nuclear envelope rupture drives genome
703 instability in cancer. *Mol. Biol. Cell* **27**, 3210-3213. doi: 10.1091/mbc.E16-02-0098
704 (2016).
705 49. Halfmann, C. T., Sears, R. M., Katiyar, A., Busselman, B. W., Aman, L. K., Zhang,
706 Q., O'Bryan, C. S., Angelini, T. E., Lele, T. P., & Roux, K. J. Repair of nuclear
707 ruptures requires barrier-to-autointegration factor. *J. Cell Biol.* **218**, 2136-2149. doi:
708 10.1083/jcb.201901116 (2019).
709 50. Chiu, Y. H., Macmillan, J. B., & Chen, Z. J. RNA polymerase III
710 detects cytosolic DNA and induces type I interferons through the RIG-I pathway.
711 *Cell* **138**, 576-91. doi: 10.1016/j.cell.2009.06.015 (2009)
712 51. Sun, L., Wu, J., Du, F., Chen, X., & Chen, Z. J. Cyclic GMP-AMP synthase is
713 a cytosolic DNA sensor that activates the type I interferon pathway. *Science* **339**,
714 786-91. doi: 10.1126/science.1232458 (2013).

715 52. Burdette, D. L., Monroe, K. M., Sotelo-Troha, K., Iwig, J. S., Eckert, B., Hyodo,
716 M., Hayakawa, Y., & Vance, R. E. STING is a direct innate immune sensor of
717 cyclic di-GMP. *Nature* **478**, 515-8. doi: 10.1038/nature10429 (2011).
718 53. Takaoka, A., Wang, Z., Choi, M. K., Yanai, H., Negishi, H., Ban, T., Lu, Y.,
719 Miyagishi, M., Kodama, T., Honda, K., Ohba, Y., & Taniguchi, T. DAI (DLM-
720 1/ZBP1) is a cytosolic DNA sensor and an activator of innate immune response.
721 *Nature* **448**, 501-5. doi: 10.1038/nature06013. (2007).
722 54. Liu, C., Wang, H., Zhao, Z., Yu, S., Lu, Y.B., Meyer, J., Chatterjee, G.,
723 Deschamps, S., Roe, B. A. & Lengyel, P. MyoD-dependent induction during
724 myoblast differentiation of p204, a protein also inducible by interferon. *Mol. Cell*
725 *Biol.* **20,** 7024–7036 (2000).
726 55. Miyashita, M., Oshiumi, H., Matsumoto, M., & Seya, T. DDX60, a DEXD/H box
727 helicase, is a novel antiviral factor promoting RIG-I-like receptor-mediated
728 signaling. *Mol. Cell Biol.* **31**, 3802–3819. doi: 10.1128/MCB.01368-10 (2011).
729 56. Semenova, N., Bosnjak, M., Markelc, B., Znidar, K., Cemazar, M., & Heller, L.
730 Multiple cytosolic DNA sensors bind plasmid DNA after transfection. *Nucleic*
731 *Acids Res.* **47**, 10235-10246. doi: 10.1093/nar/gkz768 (2019).
732 57. Sears, R. M., & Roux, K. J. Diverse cellular functions of barrier-to-
733 autointegration factor and its roles in disease. *J. Cell Sci.* **133**, jcs246546. doi:
734 10.1242/jcs.246546 (2020).
735 58. Wiebe, M.S., & Jamin, A. The Barrier to Autointegration Factor: Interlocking
736 Antiviral Defense with Genome Maintenance. *J. Virol.* **90**, 3806-3809. doi:
737 10.1128/JVI.00178-16 (2016).

59. Ma, H., Qian, W., Bambouskova, M., Collins, P. L., Porter, S. I., Byrum, A. K., Zhang, R., Artyomov, M., Oltz, E. M., Mosammaparast, N., Miner, J. J., Diamond, M. S. Barrier-to-Autointegration Factor 1 Protects against a Basal cGAS-STING Response. *mBio* **11**, e00136-20. doi: 10.1128/mBio.00136-20 (2020).
60. Guey, B., Wischnewski, M., Decout, A., Makasheva, K., Kaynak, M., Sakar, M. S., Fierz, B., & Ablasser, A. BAF restricts cGAS on nuclear DNA to prevent innate immune activation. *Science* **369**, 823-828. doi: 10.1126/science.aaw6421 (2020).
61. Yorifuji, H., Tadano Y, Tsuchiya Y, Ogawa M, Goto K, Umetani A, Asaka Y, Arahata K. Emerin, deficiency of which causes Emery-Dreifuss muscular dystrophy, is localized at the inner nuclear membrane. *Neurogenetics* **1**, 135-40. doi: 10.1007/s100480050020 (1997).
62. Haraguchi, T., Koujin, T., Hayakawa, T., Kaneda, T., Tsutsumi, C., Imamoto, N., Akazawa, C., Sukegawa, J., Yoneda, Y., & Hiraoka, Y. Live fluorescence imaging reveals early recruitment of emerin, LBR, RanBP2, and Nup153 to reforming functional nuclear envelopes. *J. Cell Sci.* **113**, 779-794 (2000).
63. Harborth, J., Elbashir, S. M., Bechert, K., Tuschl, T., & Weber, K. Identification of essential genes in cultured mammalian cells using small interfering RNAs. *J Cell Sci.* **114**, 4557-65. (2001).

Acknowledgements

We are grateful to Dr. Ritsuko Sahashi and Ms. Noriko Fukuta for technical assistance for experiments, Dr. Kentaro Kogure (Tokushima University, Japan) for insightful discussion, and Dr. Ruth Kroschewski (ETH Zürich, Switzerland) for critical reading of the manuscript. This work was supported by JST CREST JPMJCR15G2 to YO and

following JSPS grants: JP17K19505 and JP18H05528 to TH; JP19K06611 to KN; JP19H05795, JP19H03394, and JP16H06280 to YO: JP17H06167 and JP15H05972 to TF; JP20H00454 and JP18H05533 to YHiraoka.

Author contributions

TH, and YHiraoka conceived and designed the experiments. TK, TS, ŞB, HO, KN, YHirano, CM, and SK performed experiments. TH, HA, YO, YC, TF, SS, and YHirano analyzed the data. All the authors contributed reagents/materials/analysis tools. TH, YHirano, HA and YHiraoka wrote the manuscript with the input from all the authors.

Competing interests

The authors declare that they have no competing interests in relation to this work.

Materials and Correspondence

Material request and correspondence should be sent to Tokuko Haraguchi (haraguchi@fbs.osaka-u.ac.jp).

780 **Figure legends**

781 **Fig. 1**. **Gene expression from foreign DNA occurs after mitosis.**

782 **a.** Schematic of the experiment. Top: diagram of pLacO-pEF1α-mRFP. This plasmid
783 carries a *lacO* repeat sequence (256 repeats, about 10 kbp) and a sequence expressing a
784 monomeric red fluorescent protein (RFP) under the EF1α promoter. Bottom left: when
785 the transfected plasmids are exposed to the cytosol upon endosome rupture, it binds to
786 GFP-LacI and becomes fluorescent. Bottom right: when it enters the nucleus,
787 expression of RFP occurs. Therefore, RFP florescence is an indication of the nuclear
788 translocation of the plasmid. While using this system, gene expression was determined
789 by the appearance of RFP fluorescence.

790 **b.** HeLa/GFP-LacI cells transfected with pLacO-pEF1α-mRFP (0.5 μg/dish)
791 diagrammed in panel a. Immediately after removal of the transfection reagent, cells
792 were fixed and immuno-stained using anti-BAF or anti-emerin antibodies. DNA
793 (stained with DAPI, blue), GFP-LacI (green), and BAF (red) or emerin (red) in the
794 merged image. Arrows indicate DAPI signals with GFP-LacI signals. Arrowheads
795 indicate DAPI signals without GFP-LacI signals. The inset shows an image with
796 increased brightness in the boxed region. Bar, 10 μm

797 **c.** Time-lapse images of transfected HeLa/GFP-LacI cells. DNA was stained with
798 Hoechst 33342. Immediately after removal of the transfection reagent, time-lapse
799 images for each wavelength were acquired at 10-min intervals (1 μm × 7 z-stacks for
800 each time-point) using DeltaVision. Maximum intensity projection images for z-stacks
801 for selected time-points are shown. The numbers represent time (h:min). Time 0
802 represents the onset of chromosome segregation. Black-and-white inverted images are

shown for each wavelength. Merged images, DNA (Hoechst 33342, blue), GFP-LacI (green), and RFP (red). Bar, 10 μm.

d. Timing of gene expression from transfected DNA. Timing of RFP expression was determined for individual cells as shown in panel (**c**). Time 0 represents the onset of chromosome segregation. Cell numbers tested were n=248 by DeltaVision and n=346 by LSM880; total number, n=594. These data are combined in this graph. M, G1, and S represent the cell cycle phases estimated based on our previous report[38].

Fig. 2. DNA puncta disperse during mitosis.

a. Representative time-lapse images of HeLa/GFP-LacI cells transfected with pLacO-pEF1α-mRFP. DNA was stained with Hoechst 33342. Immediately after removal of the transfection reagent, time-lapse images for each wavelength were acquired at 10-min intervals (1 μm × 7 z-stacks for each time-point) using DeltaVision. The z-stack images were deconvoluted. Maximum intensity projection images for the deconvoluted z-stacks of selected time points are shown. Time 0 represents the leftmost image (680 min after the start of image acquisition). Black-and-white inverted images are shown for each wavelength. Merged images, DNA (red) and GFP-LacI (green). Bar, 10 μm.

b. HeLa/GFP-LacI cells transfected with pLacO-pEF1α-mRFP, fixed and immuno-stained for emerin as indicated in Fig. 1b. A single, representative prometaphase cell is shown. The upper and lower rows show the same cell at focal planes 1.5 μm apart. Arrowheads indicate small puncta with emerin signals. Black-and-white inverted images are shown for each wavelength. Merged images, DNA (DAPI, blue), GFP-LacI (green), and emerin (red). Bars, 10 μm.

b'. Enlarged image of the lower panel of GFP-LacI in Fig.**2b**. Arrows indicates small puncta.

c. Same as panel b except that a metaphase cell is shown. Bar, 10 μm.

d. Super-resolution images of GFP-LacI and chromosomes in a metaphase cell. HeLa/GFP-LacI cells were transfected with pLacO-pEF1α-mRFP. After transfection, cells were fixed with a fixative as described in Methods. Super-resolution images were obtained using LSM880 Airyscan microscope. White and magenta represent small puncta of transfected DNA and chromosomes, respectively. Bar, 10 μm.

e. Diagrams of transfected DNA in interphase, prometaphase, and metaphase cells.

Fig. 3. CLEM images showing small puncta of transfected DNA in telophase cells. HeLa/GFP-LacI cells were transfected with pLacO-pEF1α-mRFP, fixed and subjected to indirect immunofluorescence imaging (**a**) or CLEM (**b**-**f**).

a. Indirect immunofluorescence images of telophase cells. After removal of the transfection reagent, cells were fixed and immuno-stained for emerin. DAPI (DNA, blue), GFP-LacI (green), emerin (red) are shown in the merged image. The rightmost cartoon illustrates the core (red) and non-core regions (green) of the NE forming around the telophase chromosomes. Arrows, positions of GFP-LacI. Bar, 10 μm.

b. Representative CLEM of telophase cells. Green and magenta represent GFP-LacI and DAPI signals, respectively. Left and right, fluorescence and electron microscopic images, respectively. Middle, merged image. Bar, 5 μm.

c. Electron micrographs of the yellow-boxed region of dot 1 in panel **b**. Arrows, positions of GFP-LacI marked with green. Bar, 500 nm.

d. CLEM image. Different focal planes of the cell shown in panel (**b**). Left and right, fluorescence and electron microscopic images, respectively. Middle, merged image. Arrows, positions of GFP-LacI (dots 2-4). Bar, 5 μm.

e. Higher magnification of the red-boxed region in (**d**). Red circles represent the regions of the GFP-LacI signals, marked in green. Bar, 500 nm.

f. Classification of puncta morphologies. Type 1 (cytoplasmic circle): plasmid contained within a circular structure surrounded by an NE-like membrane that is present in the cytoplasm. Type 2 (sandwich): plasmid is present between NE-like membranes. Type 3 (membrane fusion): plasmid contained in the cytoplasmic circle fused with the NE. Type 4 (attached to chromosome): plasmid attached to the telophase chromosomes. Dot 4 is the same "dot 4" shown in panel (**d**). Type 5 (inside the nucleus): plasmid inside the nucleus. Middle panels, schematics of the electron microscopic images. NE is shown as a double line. Red arrows indicate the positions of GFP-LacI, marked in green. Electron microscope images of wider areas, including the area shown in this figure, are shown in Supplementary Figure 3. Bars, 500 nm for Types 1-4 and 1 μm for Type 5.

Fig. 4. Immuno-CLEM images of telophase cells.

HeLa/GFP-LacI cells were transfected with pLacO-pEF1α-mRFP, fixed and subjected to immuno-CLEM.

a. Fluorescence images. The images on the left are overviews. DNA (stained with Hoechst 33342, blue), GFP-LacI (green), and Alexa-nanogold (red) are shown in the merged images. Right: enlarged image of the red-boxed region. Arrows 1-5 correspond to the dots analyzed in panels **b**-**e**.

b. Low-magnification electron micrograph of the telophase cell shown in panel (**a**). Blue contour, telophase chromosomal region. The right image shows merged electron and fluorescence micrographs. Arrows 1-5 indicate the positions analyzed; red-, blue-, and yellow-boxed regions are enlarged in panels **c**, **d**, and **e**, respectively. Bar, 2 μm.

c. The red-boxed region in panel **b**. Red lines, NE-like structures. Arrows, regions where the signals are concentrated. Blue line, edge of the nucleus. Nuc, Cyt, and MT label the nucleus, cytoplasm, and mitochondria, respectively. Bars, 500 nm.

d. The blue-boxed region in panel b. Red lines, NE-like structures. Arrows, regions where the signals are concentrated. Blue line, edge of the nucleus. Nuc and Cyt label the nucleus and cytoplasm, respectively. Bars, 500 nm.

e. The yellow-boxed region in panel b. Arrows, regions where the signals are concentrated. Blue line, edge of the nucleus. Nuc and Cyt label the nucleus and cytoplasm, respectively. Bars, 500 nm.

f. Diagrams of typical localizations of transfected DNA in telophase cells. Types 1-5 are classified in Fig. **3f**.

Fig. 5. Depletion of BAF delays plasmid gene expression.

a. Time-lapse images of HeLa/mClover3-mAID-Lem2 cells. HeLa/mClover3-mAID-Lem2 were transfected with pEF1α-mRFP plasmid. After removal of the transfection reagent, time-lapse images for each wavelength were acquired every 10 or 15 min (2 μm x 5 z-stacks for each time point) using DeltaVision. IAA (indole-3-acetic acid) or ethanol as a control was added to HeLa/mClover3-mAID-Lem2 cells during live-cell imaging. Maximum intensity projection images of selected time points are shown. The numbers represent time (h:min). Time 0 is the onset of chromosome segregation. Black

arrow indicates timing of the addition of IAA. Colors represent mClover3-mAID-Lem2 (green), RFP (magenta) and Hoechst 33342 (white). Orange arrows indicate timing of RFP expression. Bar, 10 μm.

b. Timing of RFP expression in control parental (control) and Lem2-depleted HeLa (IAA) cells. Timing of RFP expression was determined for individual cells as shown in panel (**a**). Time 0 is the onset of chromosome segregation. Cell numbers tested are indicated in the graph.

c. Time-lapse images of transfected HeLa cells treated with siRNA targeting *BAFN1* (iBAF) and control siRNA (iLuc). Cells were treated with siRNA (iBAF or iLuc) and transfected with pEF1α-mRFP plasmid. DNA was stained with Hoechst 33342 during transfection. Immediately after removal of the transfection reagent, time-lapse images for each wavelength were acquired at 10-min intervals (2 μm x 5 z-stacks for a single time-point) using DeltaVision. Images projected by the maximum intensity projection for z-stacks are shown. RFP expression from transfected DNA and Hoechst 33342 are shown in magenta and white, respectively. The numbers represent time (h:min). Time 0 represents the onset of chromosome segregation. Bar, 10 μm.

d. Western blotting of lysates of HeLa cells treated with siRNA targeting *BAFN1* (iBAF) and control siRNA (iLuc). Tubulin was used as a loading control.

e. Timing of RFP expression in HeLa cells treated with iBAF and iLuc. Timing of RFP expression was determined for individual cells as shown in panel (**c**). Time 0 represents the onset of chromosome segregation. Cell numbers tested are indicated in the graph.

Fig. 6. NE rupture causes premitotic gene expression.

a. HeLa cells were transfected with pEF1α-mRFP plasmid. NE was ruptured with a microinjection needle by microinjecting FITC-dextran into the nucleus. Left, microinjected cells (green) marked with FITC-dextran. Right, representative image of microinjection needle used for NE rupture. Bar, 10 μm.

b. Time-lapse images of cells with NE rupture shown in (**a**). Immediately after NE rupture, time-lapse images for each wavelength were captured every 10 min (2 μm x 5 z-stacks for a single time-point) using DeltaVision. Images projected by the maximum intensity projection for z-stacks are shown. From the left, FITC-dextran, RFP, and Hoechst images are shown. Black-and-white inverted images are shown for each wavelength. Merged images (second column from the right), FITC-dextran (green), RFP (red), and Hoechst 33342 (blue). The cell in the red-boxed region is shown in the lower panels. The numbers represent time (h:min) from the start of imaging. Red arrow indicates the start of RFP expression. G1, S, G2, and M represent the cell cycle phases estimated based on our previous report[38]. Bars, 10 μm.

c. Western blotting of HeLa cells treated with siRNA targeting *EMD* (iemerin) and the control (iLuc), showing that emerin expression in the cells treated with siRNA was reduced to 17% of control levels.

d. Time-lapse images of the cells treated with iemerin. HeLa cells were treated with siRNA targeting *EMD* (iemerin). The cells were transfected with pEF1α-mRFP plasmid. After transfection reagent was replaced with the culture medium, time-lapse images for each wavelength were collected every 10 min (2 μm x 5 z-stacks for a single time-point) using DeltaVision. Images projected by the maximum intensity projection for z-stacks are shown. The numbers represent time (h:min) from the start of imaging. Expression of RFP started in pre-mitotic cells (white arrow). White arrow indicates the

944 start of RFP expression. S, G2 and M represent the S, G2 and M phases of the cell

945 cycle. Bar, 10 μm.

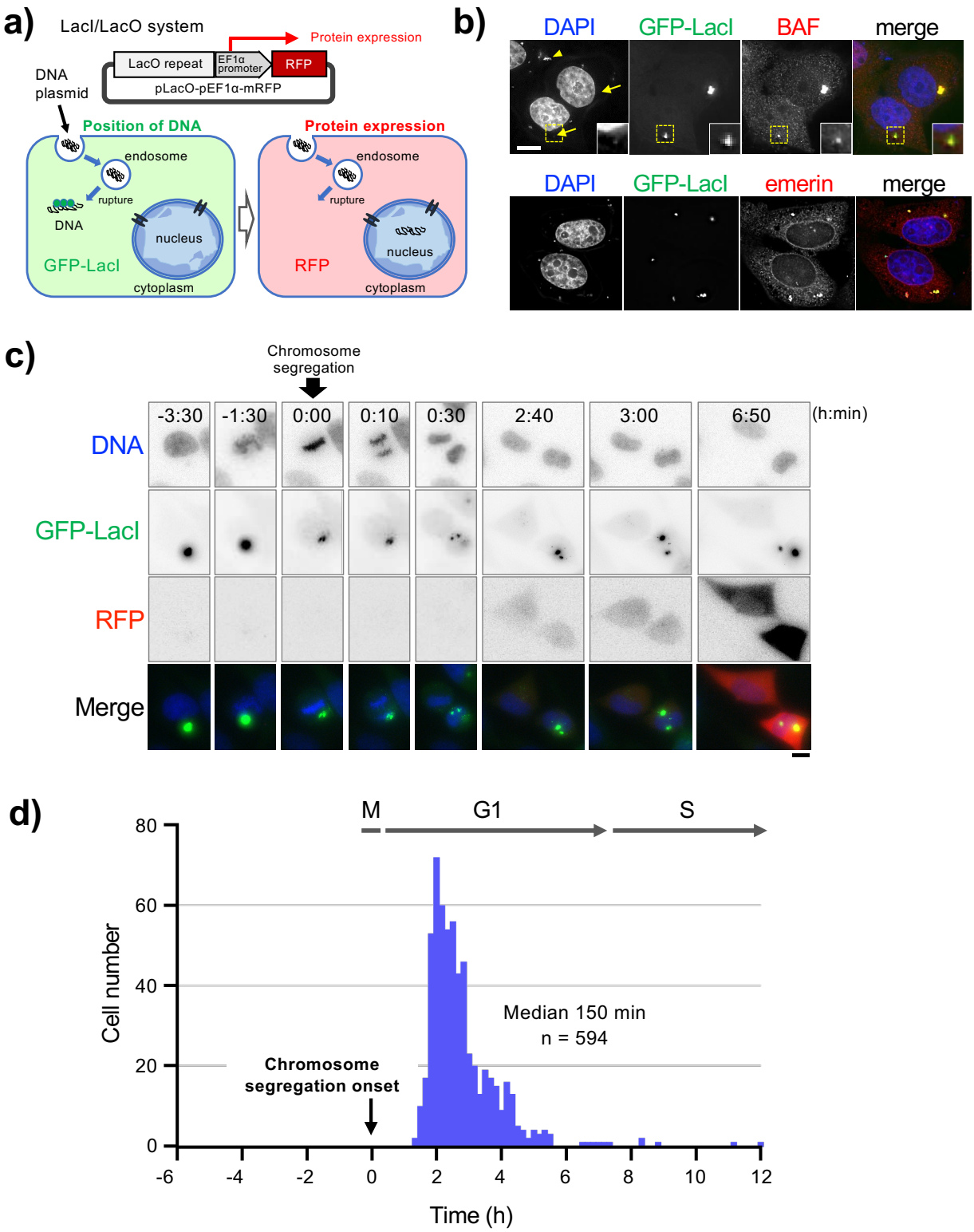

Fig. 1. Gene expression from foreign DNA occurs after mitosis.

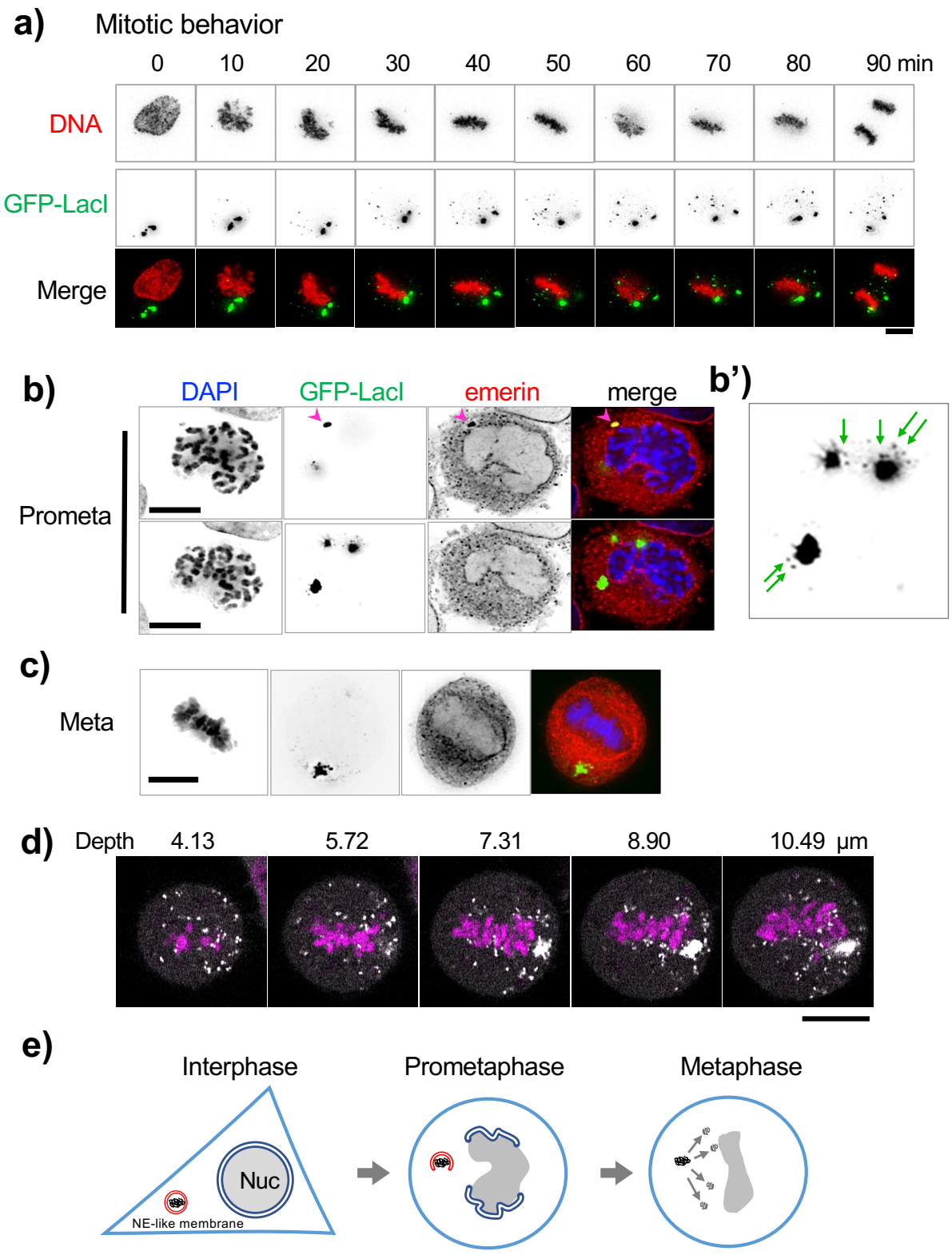

Fig. 2. DNA puncta disperse during mitosis.

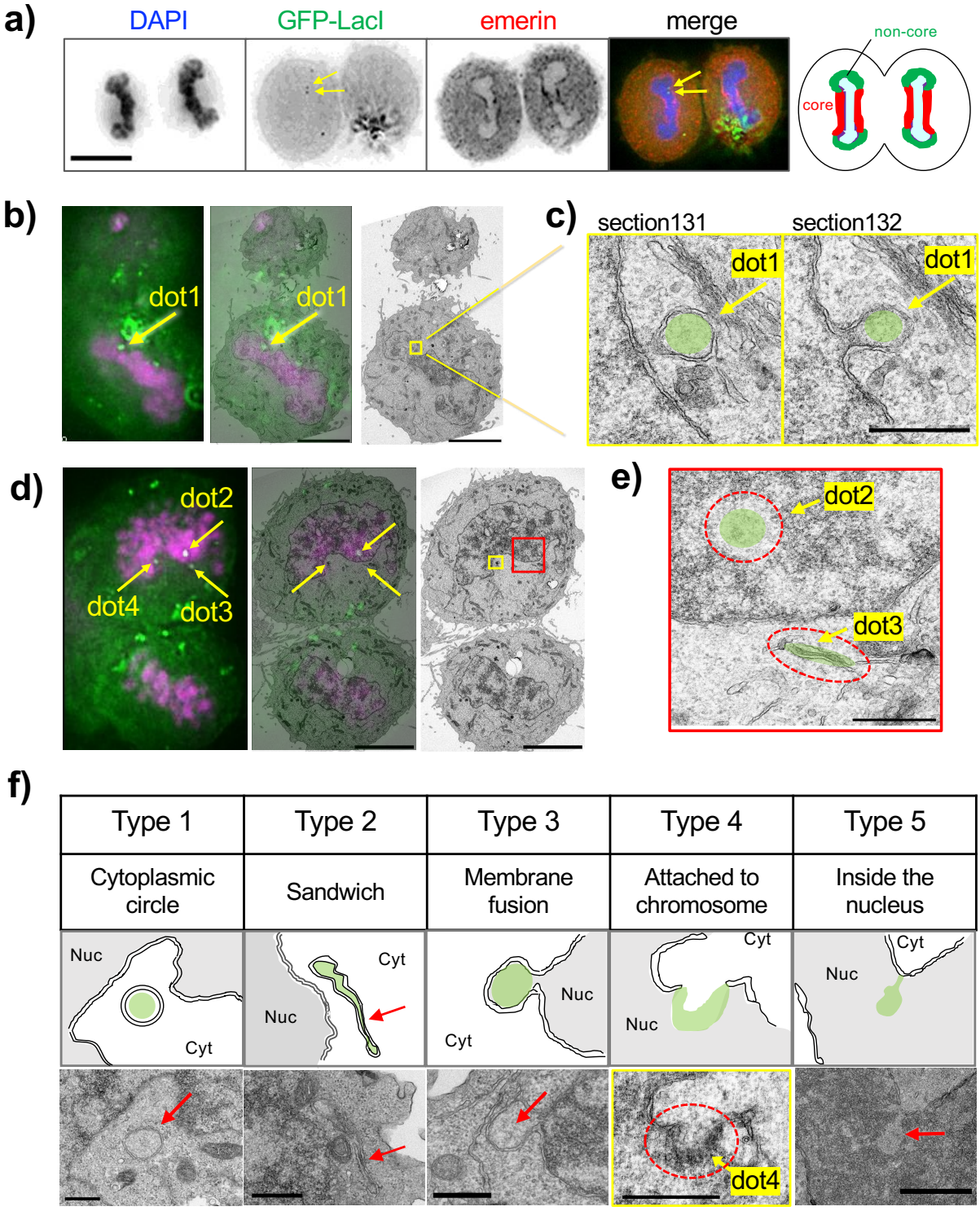

Fig. 3. CLEM images showing small puncta of transfected DNA in telophase cells.

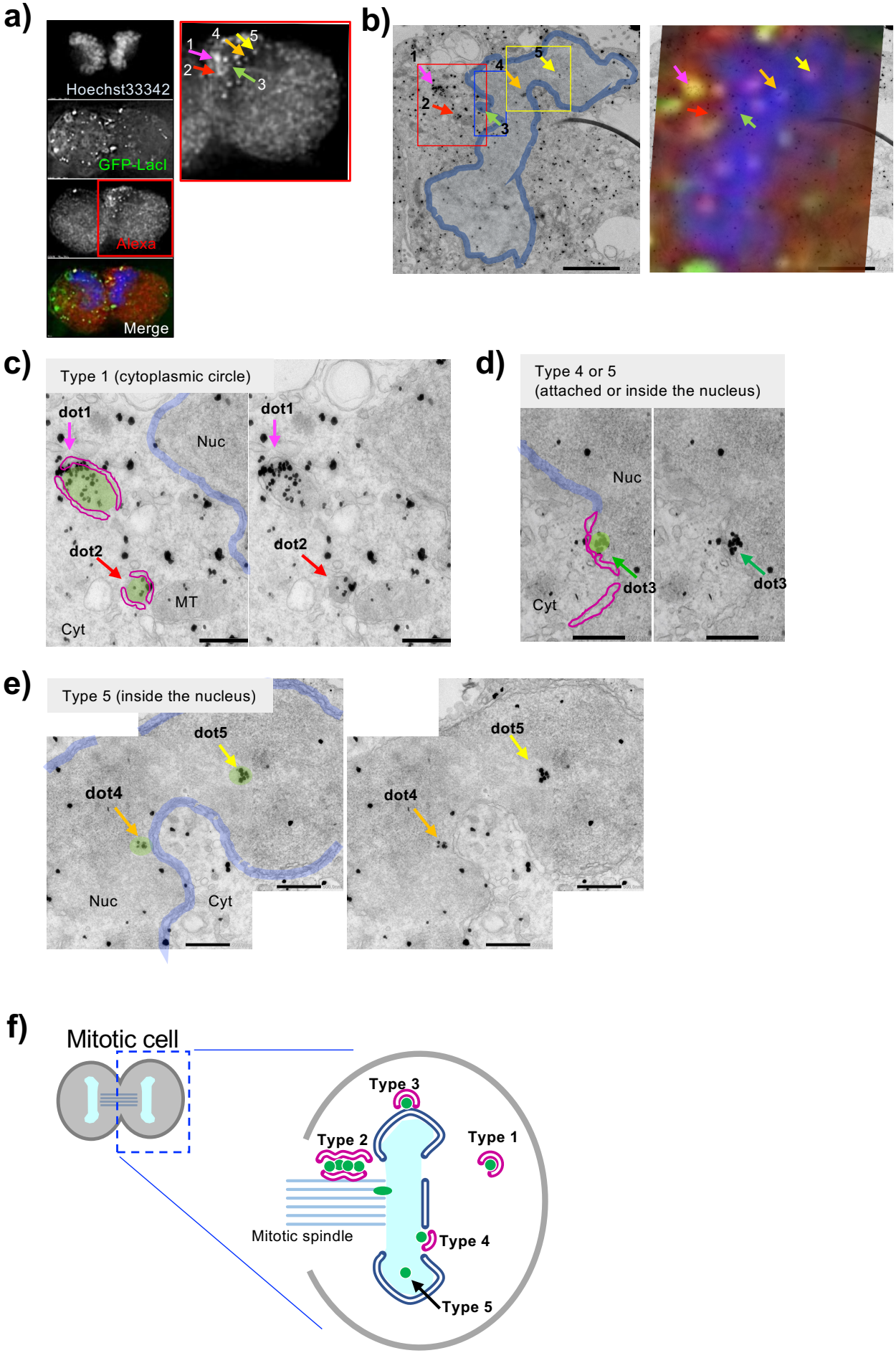

Fig. 4 Immuno-CLEM images in telophase cells

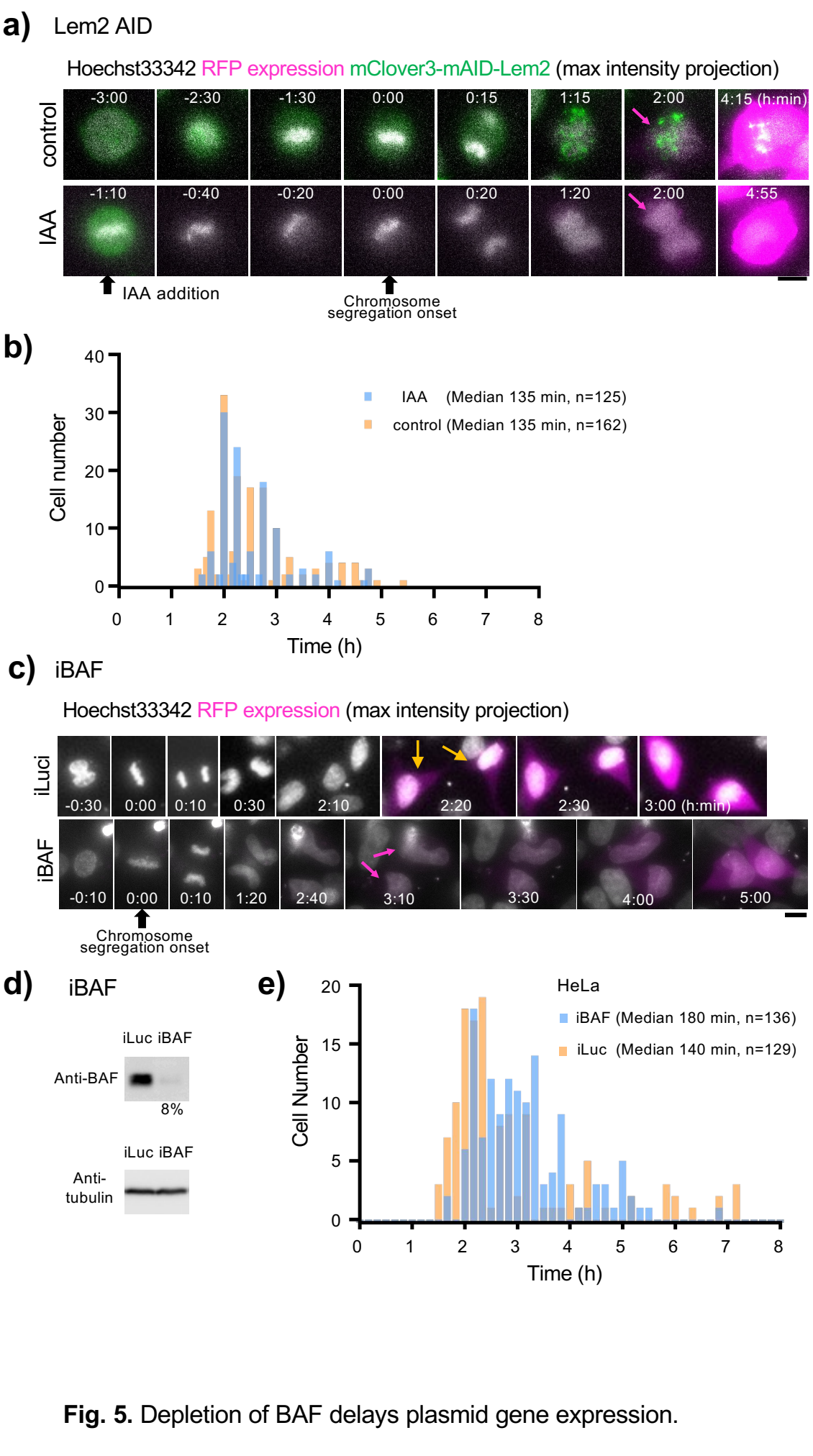

Fig. 5. Depletion of BAF delays plasmid gene expression.

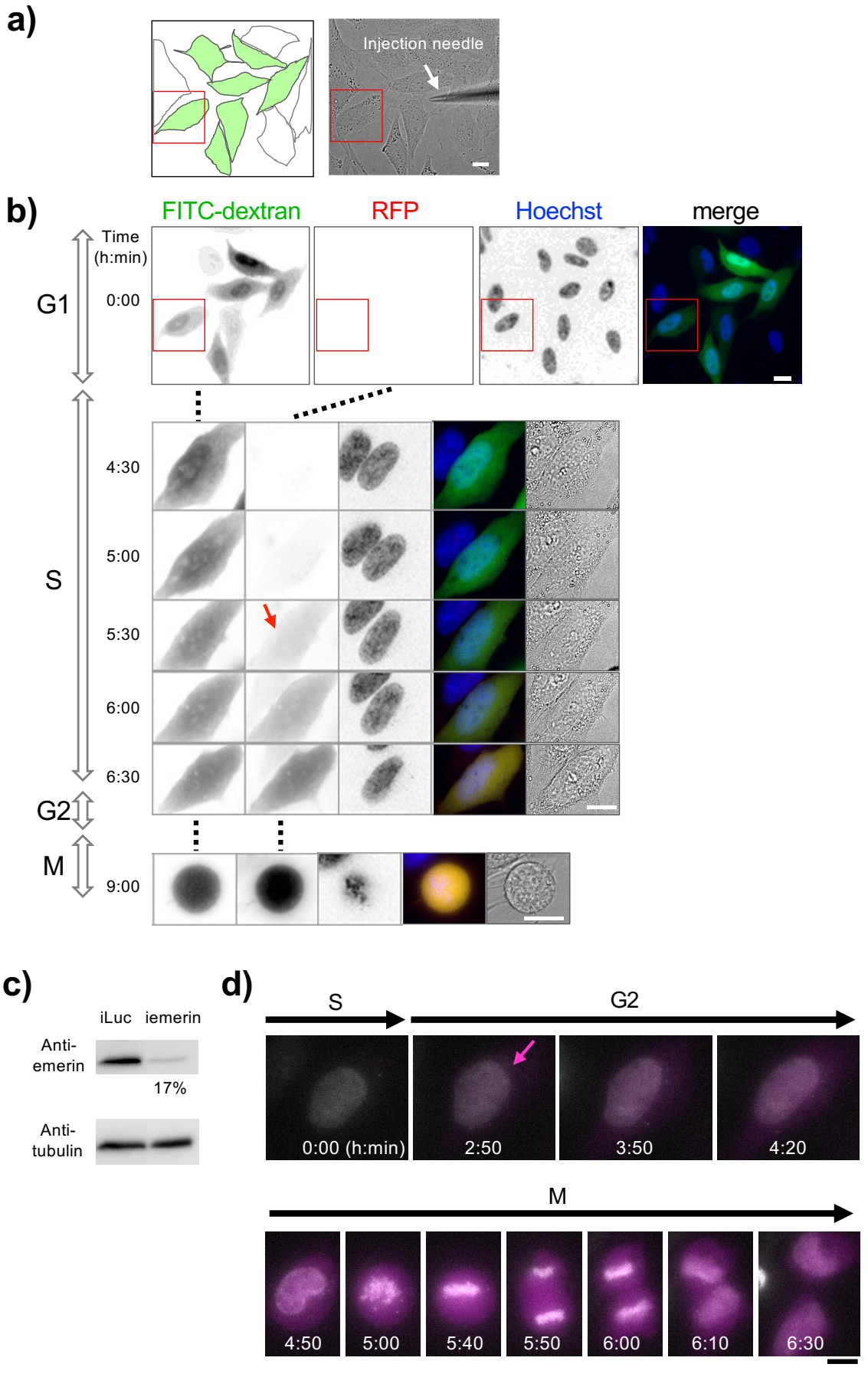

Fig. 6. NE rupture causes premitotic gene expression.

Supplementary Files

This is a list of supplementary files associated with this preprint. Click to download.

- HaraguchiSupfinal.pdf
- SourceSupFig1U2OS.xlsx
- SourceFig1dTimeExpRFP.xlsx
- SourceFig5bTimeExpAIDLem2.xlsx
- SourceFig5eTimeExpiBAF.xlsx
- SourceSupFig6bGFPiBAF.xlsx
- SourceSupFig6eiemerin.xlsx
- Haraguchisupmovie1.mov
- Haraguchisupmovie2.avi
- Haraguchisupmovie3.mov
- Haraguchisupmovie4.mov
- Haraguchisupmovie5.mov